Stem Cell Reports
Article

ISSCR

OPEN ACCESS

Generation of Induced Neuronal Cells by the Single Reprogramming Factor ASCL1

Soham Chanda,[1,2,5] Cheen Euong Ang,[1,3,5] Jonathan Davila,[1,5] ChangHui Pak,[2] Moritz Mall,[1] Qian Yi Lee,[1,3] Henrik Ahlenius,[1] Seung Woo Jung,[1,4] Thomas C. Südhof,[2,*] and Marius Wernig[1,*]

[1]Institute for Stem Cell Biology and Regenerative Medicine and Department of Pathology
[2]Department of Molecular and Cellular Physiology and Howard Hughes Medical Institute
[3]Department of Bioengineering
[4]Department of Biology
Stanford University, Stanford, CA 94305, USA
[5]Co-first author
*Correspondence: tcs1@stanford.edu (T.C.S.), wernig@stanford.edu (M.W.)
http://dx.doi.org/10.1016/j.stemcr.2014.05.020

SUMMARY

Direct conversion of nonneural cells to functional neurons holds great promise for neurological disease modeling and regenerative medicine. We previously reported rapid reprogramming of mouse embryonic fibroblasts (MEFs) into mature induced neuronal (iN) cells by forced expression of three transcription factors: ASCL1, MYT1L, and BRN2. Here, we show that ASCL1 alone is sufficient to generate functional iN cells from mouse and human fibroblasts and embryonic stem cells, indicating that ASCL1 is the key driver of iN cell reprogramming in different cell contexts and that the role of MYT1L and BRN2 is primarily to enhance the neuronal maturation process. ASCL1-induced single-factor neurons (1F-iN) expressed mature neuronal markers, exhibited typical passive and active intrinsic membrane properties, and formed functional pre- and postsynaptic structures. Surprisingly, ASCL1-induced iN cells were predominantly excitatory, demonstrating that ASCL1 is permissive but alone not deterministic for the inhibitory neuronal lineage.

INTRODUCTION

Transcriptional programs are believed to maintain cellular identities and are stabilized through various mechanisms, including chromatin modifications and lineage-determining transcription factors (Vierbuchen and Wernig, 2012). However, under several experimental approaches, imposed changes in the intrinsic and extrinsic cues have been shown to overcome these epigenetic barriers, driving the cells to pluripotency or completely unrelated somatic lineages (Jaenisch and Young, 2008; Ladewig et al., 2013; Vierbuchen and Wernig, 2011). Lineage conversion of embryonic stem cells (ESCs) and induced pluripotent stem cells (iPSCs) or already differentiated somatic cells into other cell types, such as neuronal cells, has recently attracted immense interest due to its possible application in the therapy of developmental diseases and in regenerative medicine (Blanpain et al., 2012; Han et al., 2011; Marchetto and Gage, 2012). We initially reported that forced expression of the three transcription factors ASCL1, BRN2, and MYT1L (BAM factors) successfully converts mesodermal fibroblasts into induced neuronal (iN) cells (Vierbuchen et al., 2010). In subsequent studies, we and others generated functional iN cells from human fibroblasts based on the same three BAM factors but adding additional transcription factors, microRNAs, or small molecules (Caiazzo et al., 2011; Ladewig et al., 2012; Pang et al., 2011; Pfisterer et al., 2011; Yoo et al., 2011). Thus, just like the critical breakthrough for generating iPSCs, a combination of factors was thought to be required for iN cell reprogramming from fibroblasts, and use of single transcription factors was considered insufficient.

For ESCs, on the other hand, we and others recently established that single factors, such as neurogenic differentiation factor 1 (NEUROD1) or neurogenin 2 (NGN2), alone are sufficient to rapidly induce the neuronal fate (Thoma et al., 2012; Zhang et al., 2013). In fibroblasts, however, we had originally observed that ASCL1 can induce neuronal cells only with very immature features, suggesting that single factors may initiate, but cannot complete, the reprogramming process (Vierbuchen et al., 2010). This raised interesting questions about the capacity and relative contribution of reprogramming factors toward neurogenesis from different cellular lineages. Our recent studies suggested a clear hierarchical role of the reprogramming factors, as ASCL1 alone, of the three BAM factors, immediately and directly accessed the majority of its cognate target sites in the fibroblast chromatin as a pioneer factor (Wapinski et al., 2013). BRN2 and MYT1L, on the other hand, bind to ectopic sites in a tight cell-context-specific manner and appear to be mainly required at later reprogramming stages. This suggests that ASCL1 might be the central driver of iN cell reprogramming, but it remained unclear whether ASCL1 is sufficient to induce generation of mature iN cells without further assistance from BRN2 and MYT1L.

In the present study, we addressed this very question and found that ASCL1 alone is indeed fully capable of converting mouse and human fibroblasts and ESCs into iN cells. Although ASCL1-induced single-factor neuron (1F-iN) cells displayed slower maturation kinetics at early developmental stages, their functional properties and neuronal gene-expression profile at later time points were surprisingly similar to that of NGN2- or BAM-mediated iN cells.

RESULTS

ASCL1 Alone Is Sufficient to Convert Mouse Embryonic Fibroblasts into iN Cells with Active Membrane Properties

We have previously reported that the combined expression of BRN2, ASCL1, and MYT1L (BAM) is sufficient to convert mouse fibroblasts into functional iN cells and that omission of any of the three factors yields functionally more immature cells under the conditions analyzed (Vierbuchen et al., 2010). However, we recently observed that ASCL1 acts as an "on target" pioneer factor, whereas BRN2 and MYT1L appear to engage with the fibroblast chromatin less robustly and in a much more context-dependent fashion (Wapinski et al., 2013). This raised the question whether ASCL1 is also functionally the main driver of iN cell formation and whether ASCL1 alone might be sufficient to generate mature iN cells. To address this question, we derived mouse embryonic fibroblasts (MEFs) from TauEGFP knockin mice expressing enhanced GFP (EGFP) from the well-characterized, neuron-specific *Tau* locus (Tucker et al., 2001) and infected them with lentivirus overexpressing ASCL1 under the doxycycline-inducible Tet-on promoter. We confirmed our previous observation that ASCL1 alone induced neuronal features and detected cells with bright TauEGFP fluorescence but immature morphologies 7 days after transduction (Vierbuchen et al., 2010; Figure 1A, left panel).

Next, we wondered whether improved and extended culture conditions would be sufficient to complete the reprogramming of ASCL1-only iN cells. It is well established that glial cultures provide critical trophic support for neurons and are essential for synapse formation (Baloh et al., 2000; Clarke and Barres, 2013; Wu et al., 2006). Remarkably, the coculture with glia for another 2 weeks was sufficient to turn immature ASCL1-induced 1F-iN cells into neuronal cells with very elaborate neuronal morphologies (Figure 1A, middle and right panels). In order to determine whether these cells have membrane properties characteristic of functional neurons, we performed patch-clamp recordings of TauEGFP-positive cells on days 7, 14, and 21 after infection. We observed a progressive increase in membrane capacitance and decrease of membrane resistance and resting membrane potential during this time frame, as one would expect from maturing neurons (Figure 1B). Also, voltage-gated Na^+/K^+ currents continued to increase over time (Figure 1C), and action-potential (AP) firing properties in terms of AP number, threshold, and height matured substantially from days 7 to 21 (Figure 1D). Finally, by day 21 after induction, 1F-iN cells also expressed mature neuronal markers (Figure 1E). These data show that the single factor ASCL1 alone is sufficient to convert MEFs into iN cells with intrinsic membrane properties of mature neurons when the cells are cultured in optimized conditions.

The Reprogramming Function of ASCL1 Is Unique among the Proneural bHLH Family of Transcription Factors

The family of proneural basic helix-loop-helix (bHLH) transcription factors consists of many closely related genes that are well conserved throughout the animal kingdom (Bertrand et al., 2002). Some bHLH factors are early expressed during neuronal induction, while others are expressed at later stages of neuronal maturation (Cau et al., 2002; Helms et al., 2005). Typically, early and late bHLH factors exhibit a region-specific expression pattern, suggesting that their proneural or promaturation functions are conserved. For example, of the early bHLH factors, ASCL1 is most strongly expressed ventrally in the forebrain, whereas NGN1 and NGN2 are expressed dorsally (Guillemot et al., 1993; Lo et al., 1991). Genetic deletion of NGN2 leads to a dorsal upregulation of ASCL1, which is considered to compensate for the loss of proneural NGN2 function in this area (Fode et al., 2000). Genetic switching experiments between ASCL1 and NGN2 have only uncovered subtle functional differences between the two genes (Parras et al., 2002).

We therefore asked whether the closely related proneuronal bHLH transcription factors NGN2 and NEUROD1 could replace ASCL1 and induce neuronal cells from MEFs as single factors. Of note, both genes are powerful inducers of the neuronal fate in mouse and human pluripotent stem cells (Sugimoto et al., 2009; Thoma et al., 2012; Zhang et al., 2013). Surprisingly, only ASCL1, but neither NGN2 nor NEUROD1, was able to generate any TauEGFP-positive cells from MEFs (Figure 2A). This finding suggests that one or more critical ASCL1 downstream target genes fail to be induced by NGN2. To test this hypothesis, we measured the endogenous mRNA levels of *Brn2* and *Myt1l* in transitioning MEFs 7 days after ASCL1 and NGN2 induction, using quantitative RT-PCR (Figure 2B). We found a strong and consistently higher *Myt1l* mRNA expression as well as a moderate enhancement of *Brn2* mRNA levels in ASCL1-induced MEF iN cells, when compared to NGN2 (Figure 2B; Figure S1 available online). Next, we asked whether the differential induction of *Myt1l* and/or *Brn2* could explain the

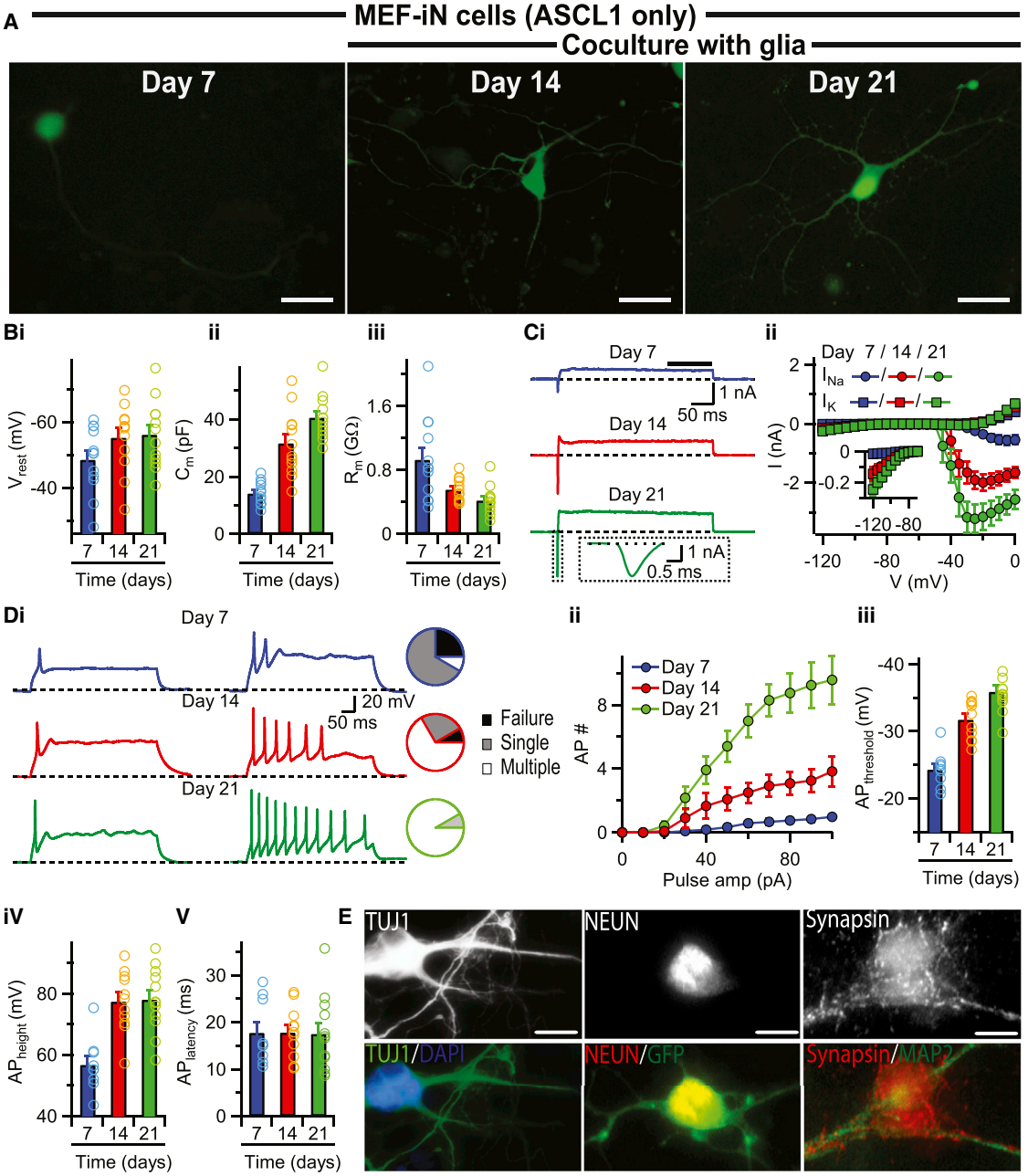

Figure 1. ASCL1 Alone Is Sufficient to Generate Functional 1F-iN Cells from MEFs

(A) Representative images displaying gradual development of the morphological complexity of ASCL1-induced single-factor MEF-iN cells at day 7 (left) and after coculturing with glia until day 14 (middle) or day 21 (right). Scale bars, 10 μm.

(B) Average values of resting membrane potential (V_{rest}, i), membrane capacitance (C_m, ii), and input resistance (R_m, iii) of ASCL1-induced single-factor MEF-iN cells from day 7 (blue), day 14 (red), and day 21 (green). Bar graphs represent mean values ± SEM (n = 12 for individual averages). Open circles of corresponding colors represent values measured from individual cells.

(C) Example traces of Na^+/K^+ currents recorded at $V_{hold} = -70$ mV with a step voltage of 50 mV (i) and corresponding averages ± SEM (n = 12 for each point, ii) for current-voltage (I-V) relationship (filled circles: Na^+-current and filled squares: K^+-current) recorded from single-factor MEF-iN cells at day 7 (blue), day 14 (red), and day 21 (green). The black line (upper panel, i) indicates time period used for calculating average K^+ currents. The insets depict expanded views of Na^+ current (bottom panel, i) and reversal of K^+ current (ii).

(D) Analysis of action potential (AP) firing properties from 1F-iN cells at day 7 (blue), day 14 (red), and day 21 (green). Example traces of single (left) or multiple (right) APs generated by a 90 pA step-current injection, with pie charts representing fraction of iN cells in each

(legend continued on next page)

differential effects of ASCL1 and NGN2 in MEFs. Indeed, supplementing NGN2-induced MEF cells with MYT1L and BRN2 or even with MYT1L alone overexpression was sufficient to generate functional iN cells (Figure S1). These findings suggest that MYT1L is a critical mediator of iN cell reprogramming that cannot be induced by NGN2 alone.

ASCL1-iN Cells Can Reach Maturation Levels Equivalent to Those of BAM-iN Cells

We previously found that ASCL1-iN cells were less mature than BAM-iN cells 12 days after induction in the absence of glia, based on intrinsic active membrane properties (Vierbuchen et al., 2010). Therefore, we next asked whether prolonged coculture with glia would allow generation of 1F-iN cells of a maturation state similar to that of BAM-iN cells. Qualitative assessment of morphological properties revealed vast differences between the ASCL1 and BAM infection on day 7 but suggested a similar complexity of neuronal shapes with similar neurite numbers and complexity on day 21 (Figure 2C). In order to quantify the degree of maturation, we compared eight electrophysiological parameters (membrane capacitance, input resistance, resting membrane potential, AP number, AP threshold, AP height, and peak Na^+ and K^+ currents) between ASCL1- and BAM-iN cells (Figure 2D). We measured these parameters at 7, 14, and 21 days after induction because we had noticed a gradual increase of maturation in both ASCL1-derived and BAM-derived MEF-iN cells during this time period (Figure 1 and Figure S2, respectively). We found that the average values of most of the parameters were significantly different on days 7 and 14 but lost statistical significance 21 days after induction. Thus, 1F-iN cells are more immature at early reprogramming stages but can reach the similar maturation state as BAM-iN cells 3 weeks after induction when cultured in optimized conditions.

1F-iN Cells Form Functional Synapses

The defining feature of neuronal identity is functional synapse formation. We therefore asked whether 1F-iN cells can receive synaptic inputs from other neurons (i.e., generate functional somatic or dendritic postsynaptic structures) and whether they can form synapses onto other neurons (i.e., generate functional axonal presynaptic structures).

To address their postsynaptic competence, we sparsely plated TauEGFP-positive 1F-iN cells 7 days after induction on previously established hippocampal neuronal cultures (2 days in vitro) and performed patch-clamp recordings from EGFP-positive cells on day 21 (Figure 3A). We readily observed both spontaneous excitatory (AMPA receptor-mediated) and inhibitory ($GABA_A$ receptor-mediated) postsynaptic currents (EPSCs and IPSCs) in 1F-iN cells, as confirmed by application of the specific AMPA and $GABA_A$ receptor antagonists CNQX and picrotoxin, respectively (Figures 3B and 3C). Furthermore, AMPA receptor- and NMDA receptor-mediated evoked EPSCs and $GABA_A$ receptor-mediated evoked IPSCs could also be elicited by extracellular field stimulation (Figures 3D and 3E), clearly indicating that 1F-iN cells can specialize postsynaptic membrane compartments and receive synaptic input from primary mouse hippocampal neurons.

To address the presynaptic functional competence of 1F-iN cells, we plated 7-day TauEGFP-positive cells in high density on a pure glial culture devoid of primary neurons and characterized them 14 days later (Figure 3F). Immunostaining experiments demonstrated that ASCL1-induced MEF iN cells express excitatory neuronal marker vesicular glutamate transporter 1 (vGLUT1), but not inhibitory neuronal marker vesicular GABA transporter (vGAT), similar to BAM-induced MEF-iN cells (Figure S3). This suggests that single-factor MEF-iN cells are predominantly excitatory. Next, we investigated whether the cells expressed functional AMPA receptors on their membranes and locally applied AMPA close to the soma and proximal dendrites of recorded iN cells. We observed AMPA receptor-mediated EPSCs with near-zero reversal potential (Figure 3G), demonstrating the presence of functional AMPA receptors in the cells even in the absence of presynaptic inputs from primary neurons. Next, we wondered whether 1F-iN cells can form functional synapses among each other. We could record both spontaneous and evoked AMPA receptor-mediated EPSCs (Figures 3H and 3I; Figure S3) as well as evoked NMDA receptor-mediated EPSCs (Figure 3I). The synapses between iN cells also displayed remarkable short-term plasticity (Figure 3I). Thus, the single transcription factor ASCL1 was capable of generating both intrinsically and synaptically mature iN cells from MEFs.

1F-iN Cells Can Be Derived from Postnatal and Human Fibroblasts

To further evaluate if 1F-iN cells can also be generated from postnatal cells, we derived tail-tip fibroblasts (TTFs) from 4-day-old TauEGFP animals. Similar to our MEF experiment,

condition able to generate single AP (gray), multiple AP (white), or no AP (black) (i). Average values presented as means ± SEM (n = 12 for individual averages) for AP number with respect to current-pulse amplitude (ii), AP threshold (iii), AP height (iv), and AP latency (v). Open circles represent corresponding values measured from individual cells (iii–v).
(E) Immunostaining analysis of 1F-iN cells at day 21 with indicated neuronal markers. Scale bars, 10 μm.

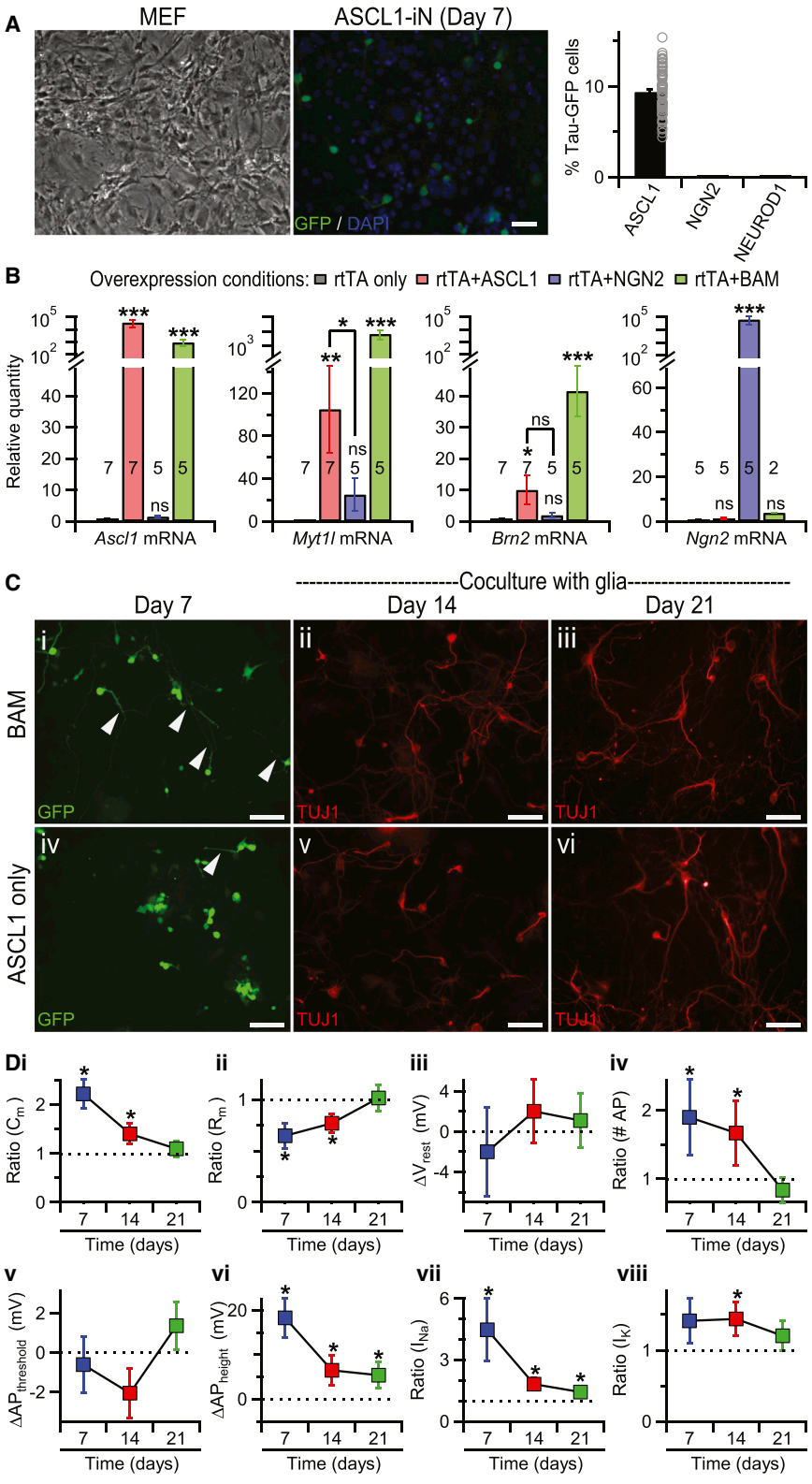

Figure 2. Delayed Maturation Kinetics of ASCL1-Induced Single-Factor MEF-iN Cells

(A) Representative images of MEFs (left) and day 7 MEF-iN cells after induction of ASCL1 transgene (middle). Immunofluorescence signals include Tau-GFP signal in green and DAPI in blue. Scale bar, 50 μm. Average percentages of TauEGFP-positive cells (right) generated using different reprogramming factors are normalized to DAPI count and plotted as means ± SEM (n = 60 fields/three batches). Open circles indicate percentages of TauEGFP-positive cells counted from individual experiments. Note that NGN2 and NEUROD1 failed to generate any TauEGFP-positive cells from MEFs.

(B) Quantitative RT-PCR for mRNA levels of *Ascl1* (left), *Myt1l* (second left), *Brn2* (second right), and *Ngn2* (right) at day 7 post-induction when MEFs were infected with lentivirus expressing rtTA only (calibration control, black), rtTA + ASCL1 (red), rtTA + NGN2 (blue), and rtTA + BAM (green). Bar graphs represent average values ± SEM, and the numbers indicate number of independent experiments for each condition. Asterisks indicate a significant difference between ΔCt_{sample} and ΔCt_{rtTA} (*$p < 0.05$, **$p < 0.01$, ***$p < 0.005$, one-tailed t test); ns, not significant ($p > 0.01$).

(C) Relative morphological comparison between BAM-induced three-factor iN cells (top) and ASCL1-induced 1F-iN cells (bottom) at day 7 (left) and after coculturing with glia until day 14 (middle) or day 21 (right). Arrowhead shows limited neurite outgrowth in immature but TauEGFP-positive iN cells at day 7. TUJ1 stainings (red) at day 14 and day 21 show gradual neurite arborization. Scale bars, 50 μm.

(D) Comparison between electrophysiological properties of BAM iN cells versus ASCL1 iN cells. Eight parameters that were compared between two conditions include membrane capacitance (C_m, i), membrane resistance (R_m, ii), resting membrane potential (V_{rest}, iii), number of APs at 90 pA current-injection step (# AP, iv), AP threshold ($AP_{threshold}$, v), AP height (AP_{height}, vi), and peak Na^+ (I_{Na}, vii) or K^+ current (I_K, viii) at −20 mV or 0 mV step-pulse, respectively. For all panels, n = 12 for day 7, n = 24 for day 14, and n = 25 for day 21. Average difference and error bars representing SEMs are generated using error propagation. Ratio represents BAM condition/ASCL1 condition, whereas Δ represents BAM condition − ASCL1 condition, for corresponding parameters. Asterisks indicate significant differences ($p < 0.05$, one-tailed t test) between the two conditions, and dotted lines indicate ratio = 1 or Δ = 0 for corresponding comparisons.

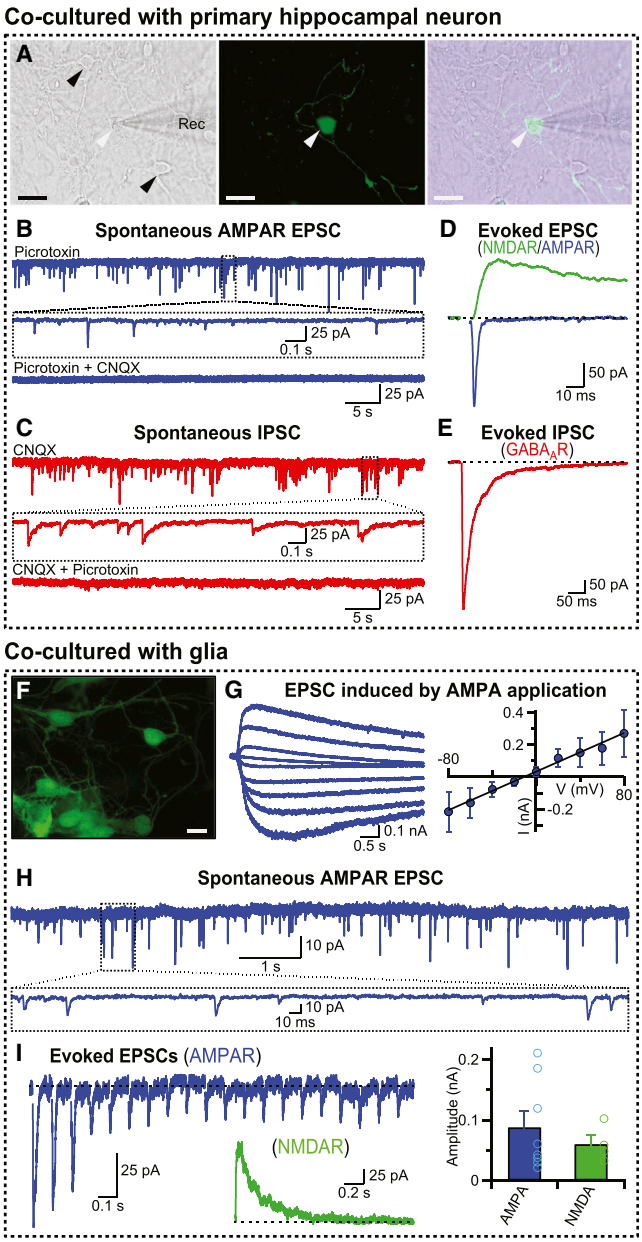

Figure 3. Functional Synapse Formation by ASCL1-Induced Single-Factor MEF-iN Cells

Electrophysiological recordings performed on ASCL1-induced 1F-iN cells cocultured with low-density primary hippocampal neurons (A–E) or with glia only (F–I).

(A) Recording configuration shown in phase contrast (left), GFP fluorescence (middle), and as both views merged (right). Rec, recording electrode; white arrowhead, TauEGFP-positive (green) 1F-iN cell; black arrowhead, hippocampal neurons (non-GFP). Scale bars, 20 μM.

(B) AMPAR-mediated spontaneous EPSCs recorded from an example cell in presence of picrotoxin (top) and blocked by subsequent application of CNQX (bottom). Expanded view of events reveals fast kinetics (middle).

(C) GABAR-mediated spontaneous IPSCs (top) with slower kinetics (middle) recorded in presence of CNQX and blocked by picrotoxin (bottom).

(D) Evoked EPSCs mediated through AMPAR (blue) and NMDAR (green), as measured from two different cells.

(E) Evoked IPSC.

(F) GFP-fluorescence view of 1F-iN cells plated on glia at a high density. Scale bar, 10 μM.

(G) EPSCs generated by puff application of AMPA at different V_{hold} (left) and average I-V plot (right) presented as means ± SEM (n = 5).

(H) AMPAR-mediated spontaneous EPSC (top) with fast kinetics (bottom) recorded from a 1F-iN cell from a pure culture.

(I) AMPAR-mediated evoked EPSCs generated with a 10 Hz train (top), and NMDAR-mediated evoked EPSC generated with a single pulse (bottom) as recorded from two different cells (left). Average (means ± SEM) peak amplitudes of AMPAR- (blue, n = 8) or NMDAR-mediated (green, n = 4) EPSCs, with values from individual cells plotted as color-matched open circles.

after coculturing with glia for 14 days (21 days postinduction), ASCL1-induced TTF-1F-iN cells displayed complex neuronal morphologies, expressed panneuronal markers, generated APs upon membrane depolarization, and exhibited Na_v/K_v-mediated currents as tested by specific blockers (Figure 4A).

Encouraged by these findings, we explored whether ASCL1 alone might be sufficient to induce iN cells even from human fibroblasts. We note that, in our experience, the conversion of human fibroblasts to iN cells is much less efficient and requires additional transcription factors (Pang et al., 2011). Surprisingly, we did indeed observe multiple TUJ1- and MAP2-positive iN cells with neuronal morphology in human fetal fibroblast (HFF; Figure 4B) and human postnatal fibroblast (HPF; Figure 4C) cultures 3 weeks after induction of ASCL1, albeit with less complex morphologies. Importantly, these HPF-derived 1F-iN cells could also generate APs (Figure 4Civ), indicating ASCL1 is also the key driver of the reprogramming process in human fibroblasts.

Generation of 1F-iN Cells from Embryonic Stem Cells with ASCL1

We and others reported that NGN2 and NEUROD1 can convert mouse and human ESCs very efficiently into iN cells (Sugimoto et al., 2009; Thoma et al., 2012; Zhang et al., 2013). In stark contrast, we had noticed that ASCL1 can induce TUJ1-positive small elongated cells from human ESCs, but these cells did not exhibit any neuronal processes up to 7 days after infection (Pang et al., 2011). Given the results of this study, we revisited the effect of ASCL1 in both mouse and human ESCs. To achieve homogeneous ASCL1 expression in mouse ESCs, we generated an

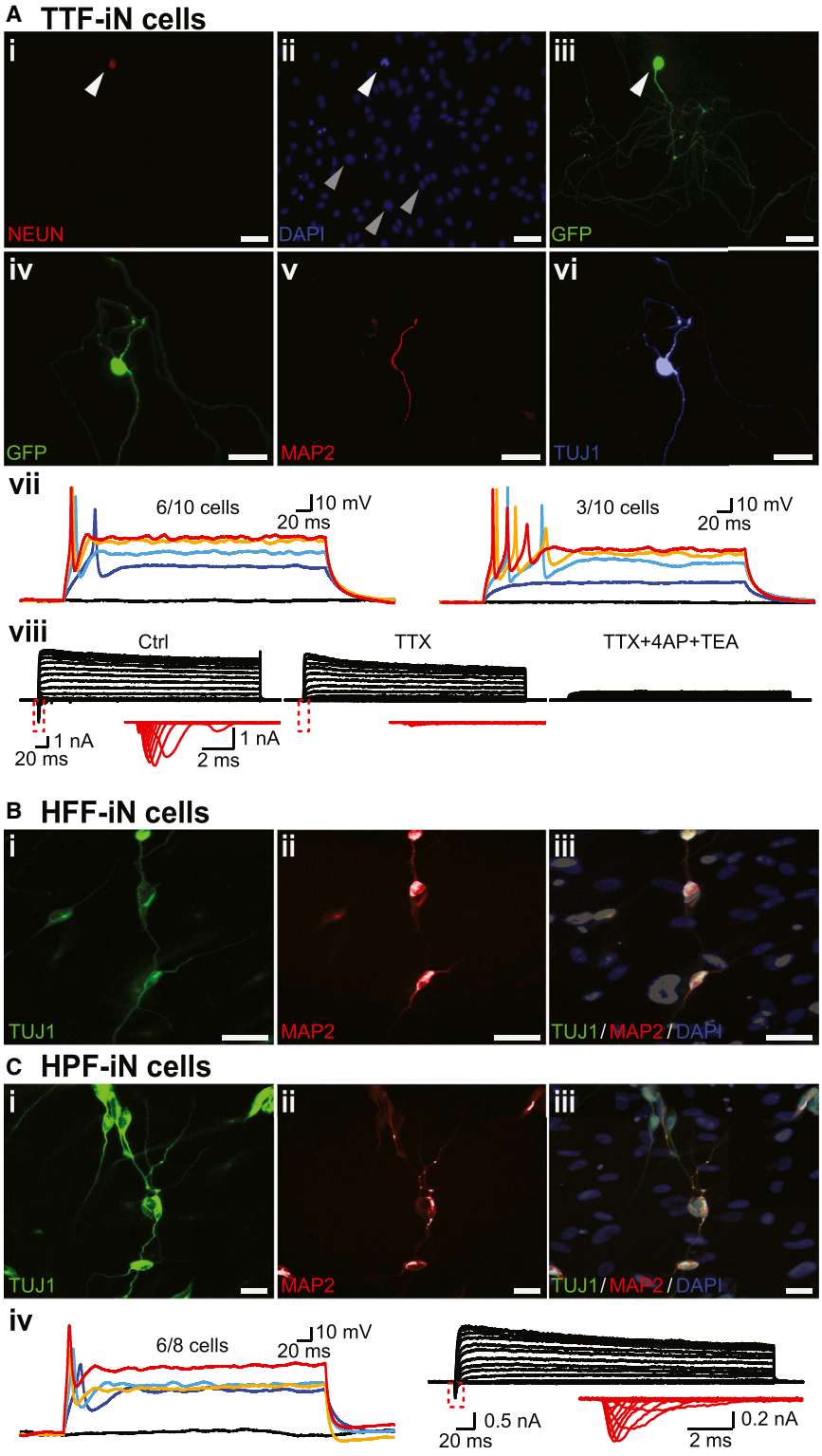

Figure 4. ASCL1 Alone Generates Functional Neurons from Postnatal Mouse and Human Fibroblast

(A) 1F-iN cells generated by ASCL1-transgene induction in tail-tip fibroblast (TTF) derived from 4-day-old animals. (A) Immunostaining of a 1F-iN cell with NEUN (i), DAPI (ii), and GFP view (iii) displaying mature neuronal morphology. White arrowhead, 1F-iN cell (i–iii); gray arrowhead, glia (ii). GFP view of a second cell (iv) immunostained for MAP2 (v) and TUJ1 (vi). Scale bars, 25 μm. Single (left) or multiple (right) AP generation by single-factor TTF-iN cells (vii) with step-current injection. Number of cells corresponding to each firing pattern is indicated. Sample traces (viii) of voltage-gated Na^+ (inset in red = magnified view of the boxed area) and K^+ currents recorded from a single-factor TTF-iN cell (left) and subsequently blocked by TTX (middle) and 4AP + TEA (right).

(B) Human fetal fibroblasts (HFF) transduced with ASCL1 and immunostained with TUJ1 (i), MAP2 (ii), and both views merged (iii) at 22 days after induction. Cells were maintained without coculturing on glia. TUJ1/MAP2-negative but DAPI-positive cells indicate nonreprogrammed fibroblasts. Scale bars, 10 μm.

(C) Similar immunostaining as (B) but performed on human postnatal fibroblast (HPF, i–iii). Scale bars, 10 μm. Example traces of AP firing (left) and voltage-gated Na^+/K^+ currents (right) recorded from single-factor HPF-iN cells (iv), similar to (A).

ASCL1-inducible mouse ESC line by simultaneous infection of doxycycline-inducible ASCL1 lentivirus and a constitutive rtTA lentivirus (Wapinski et al., 2013). Within 5 days of ASCL1 induction with doxycycline, neuronal cells with extensive neurite outgrowth were observed in this line. The neuronal cells also expressed mature

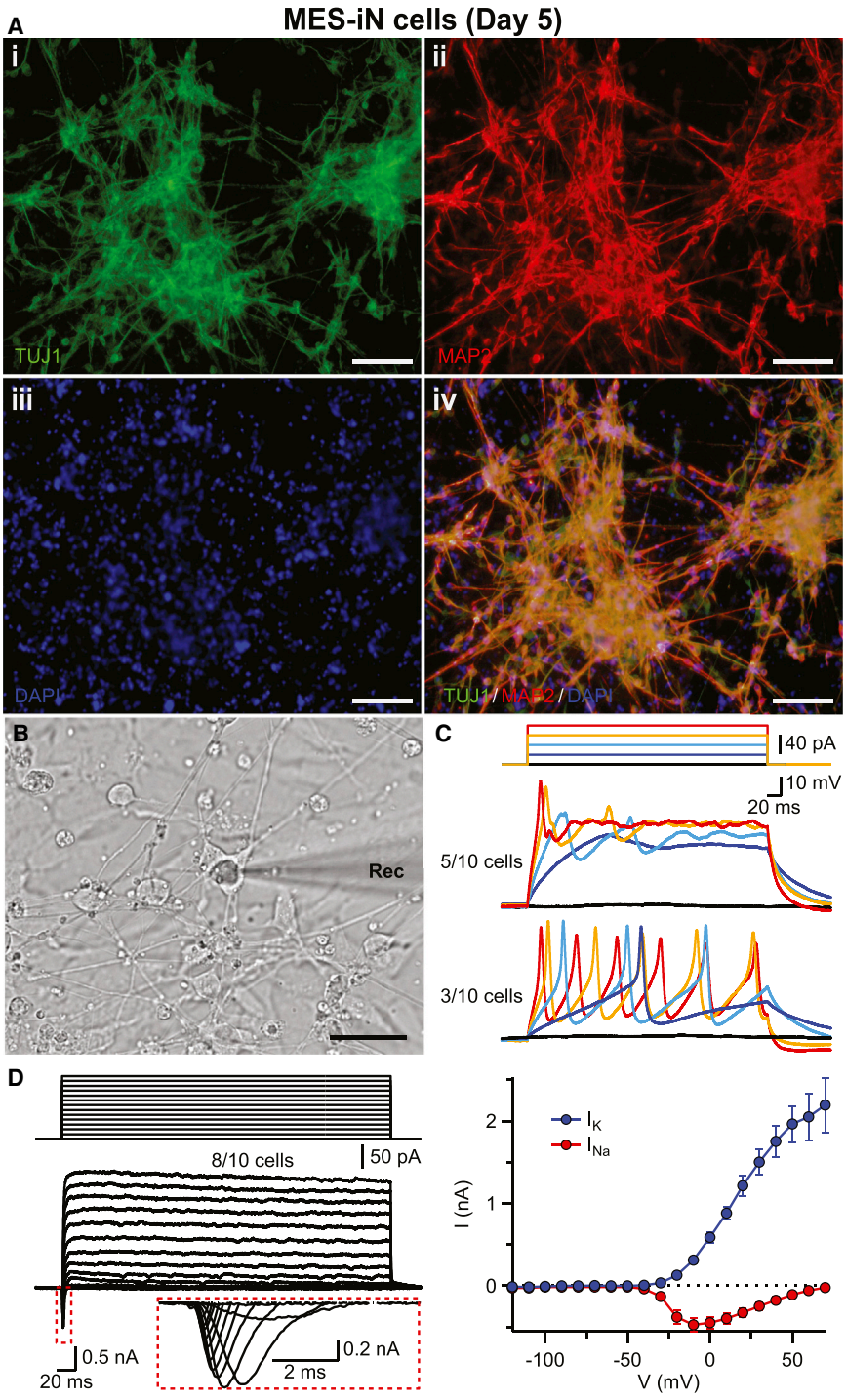

Figure 5. ASCL1 Induces Functional 1F-iN Cell Generation from Mouse Embryonic Stem Cells

(A) Mouse embryonic stem cell-derived iN (MES-iN) cells generated from ASCL1-induction and immunostained with indicated markers (TUJ1, i; MAP2, ii; DAPI, iii; and all views merged, iv). Scale bars, 100 μm.

(B) Bright-field view of MES-iN cells demonstrating patch-clamping configuration. Rec, recording electrode. Scale bar, 50 μm.

(C) Step-current (top) mediated depolarization evoked single (middle) or multiple (bottom) AP in single-factor MES-iN cells when recorded in current-clamp mode. Numbers indicate population of cells with corresponding AP firing pattern. Color codes represent responses from individual pulses.

(D) Example traces (left) representing step-voltage (top) generated inward Na^+ currents and outward K^+ currents. Inset: expanded view of Na^+ current. Average I-V curves (right) for Na^+ (I_{Na}) and K^+ (I_K) currents are plotted as mean ± SEM (n = 8 cells).

neuronal markers (Figure 5A) and were able to generate APs upon current injection (Figures 5B–5D), suggesting the successful generation of ASCL1-induced 1F-iN cells from mouse ESCs.

We next probed the ability of ASCL1 to form functional iN cells from human ESCs. H9 ESCs were infected with ASCL1-overexpressing lentivirus, treated with doxycycline to induce ASCL1, puromycin-selected, and cultured together with or without primary mouse glia (Figure 6). As seen before, without glial coculture, ASCL1-induced 1F-iN cells displayed immature morphology with inadequate neurite outgrowth on day 9, while NGN2-infected cells already

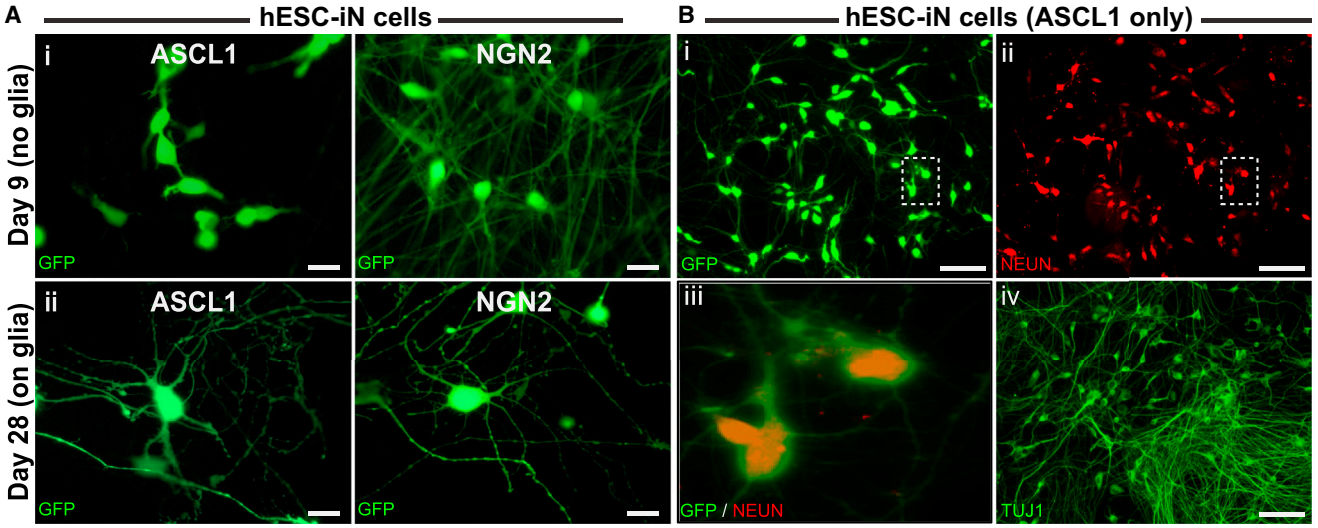

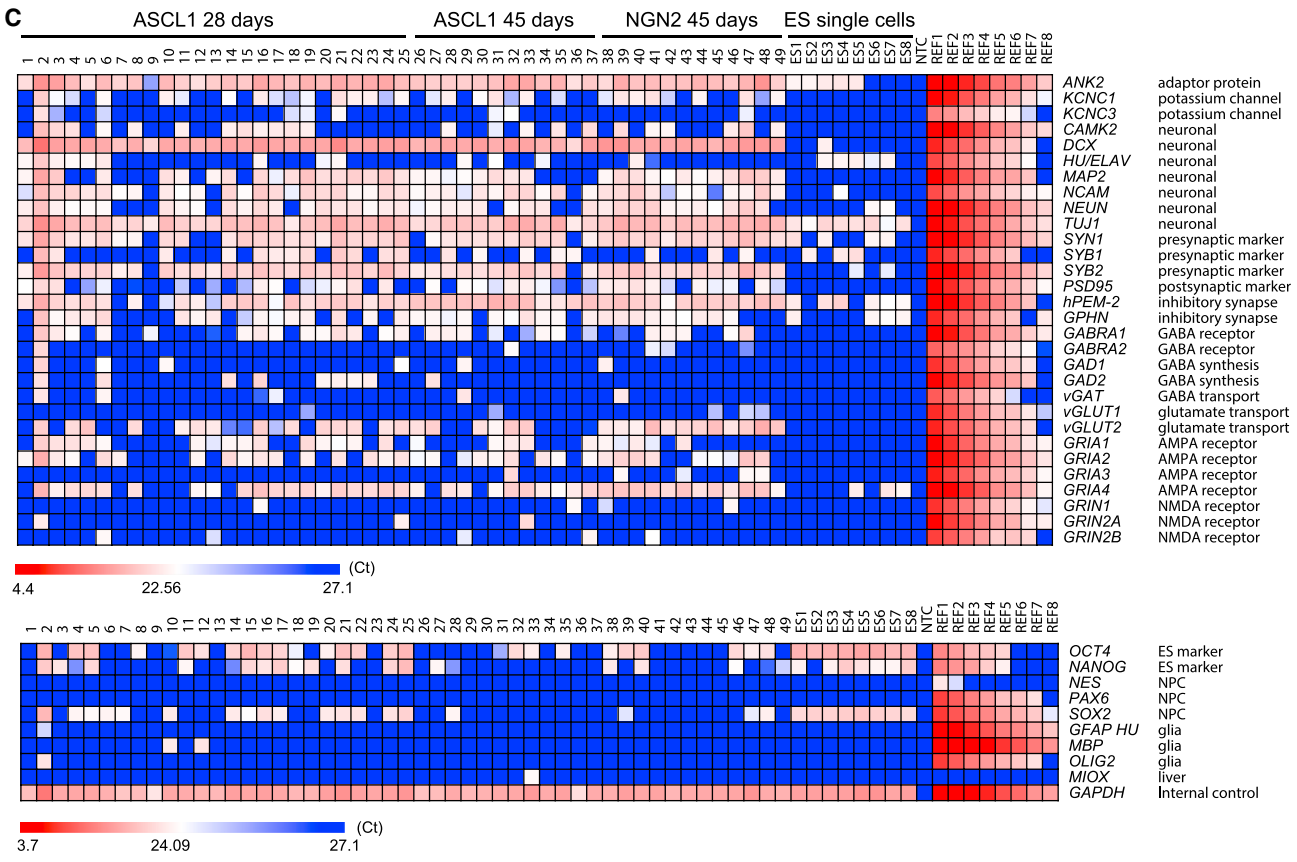

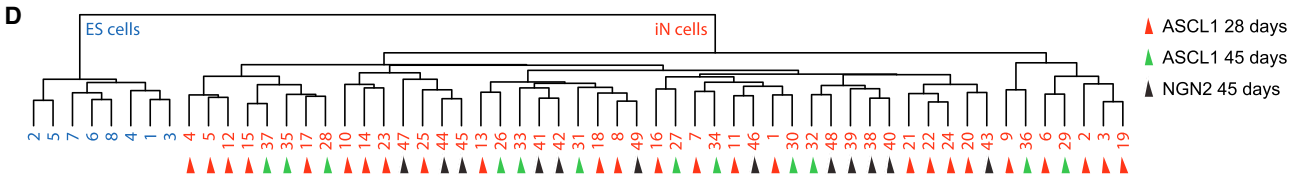

(legend on next page)

displayed mature neuronal morphologies (Figure 6A). However, after coculturing with glia for another 21 days (i.e., day 28 after infection), ASCL1-induced human ESC-derived iN (hESC-iN) cells demonstrated intricate neuronal morphologies surprisingly similar to NGN2-induced hESC-iN cells (Figure 6A). Immunofluorescence analysis showed expression of mature neuronal markers (Figure 6B). In order to more comprehensively compare the maturation state of NGN2-mediated and ASCL1-mediated hESC-iN cells, we quantified the expression levels of 31 panneuronal genes and ten nonneuronal genes at the single-cell level using the Fluidigm Biomark platform (Figure 6C). ASCL1-induced hESC-iN cells consistently expressed the mRNA levels of several panneuronal genes including cytoskeletal, ion channels, and various pre- and postsynaptic genes. The majority of the ASCL1-induced hESC-iN cells also upregulated the excitatory neurotransmitter transporter *vGLUT2*, with minimal expression of genes of the inhibitory neuronal lineages such as *Glutamic Acid Decarboxylase* (*GAD*) or *vGAT*. Although ASCL1 is classically associated with the inhibitory lineage, this marker panel surprisingly suggests that ASCL1-derived hESC-iN cells are predominantly excitatory, just like NGN2-derived ESC-iN cells and ASCL1-derived or BAM-derived fibroblast iN cells (Pang et al., 2011; Vierbuchen et al., 2010; Zhang et al., 2013; Figure 3; Figure S3). An unbiased cluster analysis based on *GAPDH*-subtracted ΔCt values (Figure 6D) further demonstrated that based on expression of these 41 genes, ASCL1- and NGN2-induced hESC-iN cells cannot be distinguished.

Finally, we asked whether the ASCL1-mediated ESC-iN cells would possess functional electrophysiological properties. Voltage-clamp recordings from these cells confirmed the presence of voltage-gated Na^+/K^+ channels and functional membrane properties of mature neurons (Figures 7A and 7B). The cells were also capable of generating mature APs upon current injection in the current-clamp mode (Figure 7C and 7D). We next probed for the synaptic competence of ASCL1-induced hESC-iN cells. Immunofluorescence stainings indicated expression of dendritic MAP2 and presynaptic SYN1 protein (Figure 7E). Additionally, puff application of exogenous AMPA and GABA demonstrated the presence of functional neurotransmitter receptors (Figure 7F). In the voltage-clamp mode, spontaneous EPSCs with fast kinetics could be readily identified (Figure 7G), and upon extracellular stimulation, evoked EPSCs could be recorded that also exhibited short-term synaptic plasticity (Figure 7H). Thus, ASCL1-induced hESC-iN cells are fully functional, predominantly glutamatergic, and indistinguishable from NGN2-induced hESC-iN cells at later stages of maturation. However, the maturation kinetics of ASCL1-induced hESC-iN cells is slower than that of NGN2-induced hESC-iN cells.

DISCUSSION

We previously found that the combined expression of three transcription factors (BAM) is required to induce fully functional iN cells from fibroblasts (Vierbuchen et al., 2010). Under the same conditions, single factors could only generate cells that had some neuronal characteristics but lacked critical others such as morphological and functional properties. Based on this observation, we had assumed that single factors can only initiate a partial reprogramming toward iN cells and additional factors are required to complete the reprogramming process. In this study, we challenged this hypothesis and demonstrate instead that cells reprogrammed with the single factor ASCL1 are in fact fully reprogrammed to a neuronal lineage but are simply less mature compared to cells reprogrammed with all three factors at early time points. Later in the reprogramming process, the single-factor iN cells can reach maturation levels almost equivalent to three-factor cells. This conclusion has important implications on how we view the molecular mechanism of iN cell reprogramming. Obviously, ASCL1 is the single most important driver of reprogramming, and success or failure of reprogramming of a given cell type

Figure 6. Comparison between ASCL1-Induced and NGN2-Induced HESC-iN Cells

(A) Morphological comparison between ASCL1 (left) and NGN2 (right) induced hESC-iN cells (GFP-infected) at day 9 (top, i) and day 28 (bottom, ii), respectively without or with culturing on glia. Note the striking difference between ASCL1 and NGN2 conditions in terms neurite arborization at day 9, but not at day 28. Scale bars, 10 μm.

(B) ASCL1-induced hESC-iN cells in GFP (i), NEUN stained (ii), and both views merged with boxed area (dotted) magnified (iii). TUJ1 staining is shown (iv) from a different plate. Scale bars, 50 μm.

(C) Quantitative RT-PCR using a Fluidigm chip, performed on cytoplasm aspirated from single iN cells by patch pipette. ASCL1- and NGN2-induced iN cells derived from H9 hESCs and collected at day 28 or day 45 after lentiviral transduction. Neuronal genes (top) and nonneuronal control genes (bottom) analyzed are indicated on the right. Expression levels (expressed as Ct values) are color-coded as shown at the bottom (color scales). Numbers indicate iN cell samples, ES1-8 indicates hESC samples (negative control), NTC indicates no template control (blank), and REF1-8 represents 7-fold dilutions of human brain total RNA (positive control).

(D) Dendrogram for cluster analysis using ΔCt values (Ct values of gene expression subtracted from that of *GAPDH*) of genes as depicted in (C). Numbers at the bottom indicate cell samples collected from the ESC (blue) or iN (red) population. iN cell identities indicated with arrowheads (red = 28 day ASCL1-induced, green = 45 day ASCL1-induced, black = 45 day NGN2-induced).

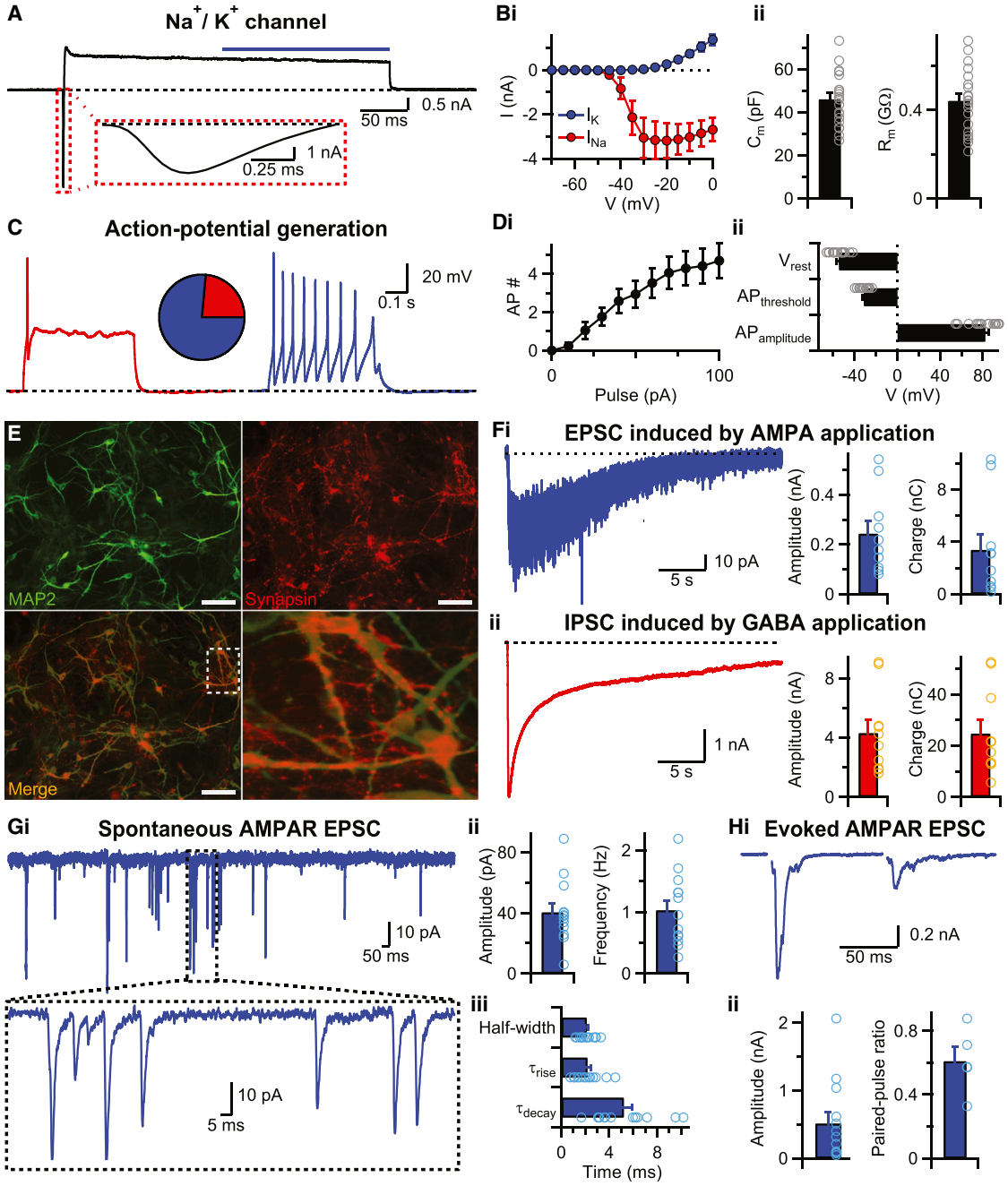

Figure 7. ASCL1-Induced Single-Factor hESC-iN Cells Display Functional Membrane and Synaptic Properties

(A) Example trace showing the presence of voltage-dependent Na^+/K^+ current. Dotted box in red points to Na^+-channel-dependent inward current, and the blue bar on top indicates time course of K^+-channel-mediated outward current used for average analysis in (B).

(B) Average (means ± SEM) current-voltage relationship (I-V curve) for Na^+/K^+ current (n = 6, i), membrane capacitance (C_m, n = 20, left, ii), and input-resistance (R_m, n = 20, right, ii). Open circles represent respective values from individual cells.

(C) Single (red) or multiple (blue) AP generation by ASCL1-induced single-factor hESC-iN cells at day 28. Pie chart indicates respective population fractions (color matched).

(D) Characterization of AP-generation properties in terms of number of APs generated with current-pulse amplitude (i), resting membrane potential (V_{rest}, ii), AP threshold ($AP_{threshold}$, ii), and AP amplitude ($AP_{amplitude}$, ii). Average values are shown as means ± SEM (n = 17), and open circles represent corresponding values from different cells.

(legend continued on next page)

will critically depend on the efficient engagement of ASCL1 with the proper chromatin targets. We recently identified an intriguing trivalent chromatin state (consisting of high H3K4 monomethylation, high H3K27 acetylation, and low H3K9 trimethylation levels) associated with ASCL1 targets in MEFs and potentially important for the correct targeting of ASCL1 to its proper sites (Wapinski et al., 2013). Now, with the knowledge that ASCL1 alone is sufficient to generate mature iN cells, these ASCL1-specific chromatin findings are even more relevant than originally assumed. In particular, for future attempts to generate iN cells from thus-far reprogramming-resistant cells such as keratinocytes or blood cells, the efforts should focus on targeting ASCL1 to its proper chromatin sites. The other two transcription factors, BRN2 and MYT1L, are not less important, but their predominant role appears to be to enhance neuronal maturation and less to contribute to the cell lineage conversion mechanism. These studies would predict that Pou-domain-containing and MYT-domain-containing transcription factors also act as maturation factors during normal neural development. Furthermore, ASCL1 can activate endogenous *Myt1l* and *Brn2* expression, which supports the notion that these two transcription factors are responsible for neuronal maturation also in ASCL1-induced iN cells.

Another remarkable observation of this study is that ASCL1-iN cells are exclusively excitatory. This is surprising, because ASCL1 is not typically associated with the excitatory neuronal lineage during neural development (Bertrand et al., 2002; Fode et al., 2000; Guillemot et al., 1993; Johnson et al., 1990; Kim et al., 2008). In the forebrain, ASCL1 is predominantly expressed in the ventral medial and lateral ganglionic eminences (Guillemot et al., 1993; Lo et al., 1991). In *Ngn2*$^{-/-}$ mice, ASCL1 is ectopically overexpressed dorsally where also inhibitory marker genes such as Dlx2 and Gad67 are induced (Fode et al., 2000). These data suggested that ASCL1 acts as an important instructive signal for the inhibitory lineage, and one might have expected that ASCL1 would induce the inhibitory neuronal lineage in fibroblasts and ESCs. However, our results clearly demonstrate that ASCL1 may be permissive for generating inhibitory neurons but alone is clearly not instructive. Its instructive function does require other factors that are present in the cellular context of a neural progenitor cell.

Our study also sheds light into the intriguing functional differences of the closely related proneural bHLH transcription factors NGN2 and ASCL1. While genetic swap experiments in vivo showed only modest factor-specific effects suggesting that both genes are functionally very similar (Parras et al., 2002), as reprogramming factors the two genes showed drastic differences. For example, in mouse fibroblasts, ASCL1 is a powerful reprogramming factor, but NGN2 alone is not able to induce neuronal features, presumably due to insufficient induction of *Myt1l*. In human ESCs, on the other hand, previous work suggested that ASCL1 is incapable of efficient neuronal reprogramming, whereas NGN2 and NEUROD1 are extremely effective in generating mature neurons within a matter of days (Pang et al., 2011; Zhang et al., 2013). It was unclear whether this mutually exclusive role is dependent of the species (mouse versus human) or the cell type (fibroblasts versus pluripotent cells). In this paper, we have clarified this question and come to the conclusion that the different effects of ASCL1 versus NGN2 are cell-context dependent. First, we report the totally unexpected finding that ASCL1 alone can indeed convert human fibroblasts to iN cells that are even able to fire mature APs. Second, we tested ASCL1 and NGN2 side by side in murine ESCs and observed that also in this condition ASCL1 induces neurons slower (about 5 days for the first appearance of neuronal morphologies) than NGN2 (about 2 days for first neuronal morphologies) (see also: Thoma et al., 2012; Yamamizu et al., 2013).

Finally, we also revised initial conclusions about the power of ASCL1 in human ESCs. Somewhat similar to the effects of ASCL1 in fibroblasts, if given more time and coculture with primary glia, ASCL1 also can induce perfectly functional and mature iN cells in human ESCs. Surprisingly though, the resulting iN cells were excitatory and based on single-cell gene expression patterns indistinguishable from NGN2-mediated ESC-iN cells. Therefore, the role of either bHLH factor for ultimate lineage specification seems very similar, but the power of proneural induction varies between the two factors depending on the cellular context. Future studies will have to be performed to identify the

(E) Immunostaining of hESC-iN cells with dendritic marker MAP2 (upper left) and synaptic marker Synapsin (upper right), merged view (bottom left), and expanded view of the dotted box (bottom right). Scale bars, 50 μm.
(F) Sample traces (left) and average values ± SEM (n = 10 for each condition) of amplitude (middle) and total charge transfer (right) for puff-induced AMPAR-mediated EPSCs (i) or GABAR-mediated IPSCs (ii).
(G) AMPAR-mediated spontaneous EPSCs (top) with boxed time-course expanded (bottom) (i). Average values of event amplitude, frequency (ii), and event kinetics in terms of half-width, rise-tau (τ_{rise}), and decay-tau (τ_{decay}) (iii) are depicted as means ± SEM (n = 13).
(H) Example trace of AMPAR-mediated EPSCs evoked by two consecutive pulses (Δt = 100 ms); stimulus artifacts are omitted for better visibility (i). Average values depicted as bar graphs (ii) representing means ± SEM for peak amplitude of evoked EPSCs (n = 13) and paired-pulse ratio (n = 5). Open circles represent values recorded from individual cells.

defining molecular features that are responsible for the different properties of these closely related genes.

EXPERIMENTAL PROCEDURES

Cell Culture and Neuronal Induction

Generation of Fibroblast-iN Cells

All experiments were carried out with the approval of the Stanford University Administrative Panel on Laboratory Animal Care (protocol 21565). MEFs or TTFs were derived from embryonic day 13.5 embryos of TauEGFP knockin mice or 4 day old WT C57/BL6 mice respectively, and cultured in MEF media for three passages, as described previously (Vierbuchen et al., 2010). Cells were infected with lentiviruses containing expression constructs of rtTA (driven by ubiquitin promoter) and ASCL1-t2a-Puro (driven by Tet-on promoter) in the presence of polybrene (8 μg/ml). For comparison with BAM iN cells (Figure 2), ASCL1-virus load was kept constant and MEF cells were coinfected with additional lentiviruses overexpressing BRN2 and MYT1L under the same Tet-on promoter. The next day, media was exchanged with fresh MEF media containing doxycycline (2 μg/ml). On day 3, media was replaced with N3 media (Dulbecco's modified Eagle's medium/F12 [Invitrogen], N2 [Invitrogen], and B27 [Invitrogen] supplemented with 12.5 mg of insulin [Sigma] and penicillin/streptomycin [Invitrogen]). For synaptic recordings or long-term culture (>7 days), cells were trypsinized (with 0.25% trypsin), pooled (i.e., two 12-well dishes into one), and replated on passage 3 mouse glia (derived from C57 pups, postnatal day 3; see Vierbuchen et al., 2010 for details) or preestablished mouse primary hippocampal neurons (2 days in vitro). Media was half-exchanged once a week.

Generation of MESC-iN Cells

A doxycycline-inducible flag-ASCL1 ESC line was established as described previously (Wapinski et al., 2013). The cells were expanded in mouse embryonic stem cell (mESC) media plus LIF in the absence of feeders. Ten million cells were seeded on a gelatin-coated 15 cm dish. The media was replaced with N3 plus doxycycline the day after seeding.

Generation of HESC-iN Cells

H9 hESCs were maintained under feeder-free conditions in mTeSR media (STEMCELL Technologies). Media was changed every day. When cell density reached 70%–80% confluence, colonies were dissociated using accutase (STEMCELL Technologies) and plated onto Matrigel (BD Biosciences)-coated plates at a 1:6 dilution. During passaging, the media was supplemented with 2 μM thiazovivin overnight. For hESC-iN formation, dissociated single cells were plated at a density of $\sim 2.5 \times 10^5$ cells per 35 mm^2 well. Lentivirus infections (with an additional EGFP-expressing virus) and transgene induction were performed similarly to as described for the fibroblast-iN production, using N3 media. Puromycin selection continued from day 2–6 postinfection, with media changes every other day. On day 7, cells were dissociated into single cells using PBS-EDTA (0.5 mM) and seeded onto mouse glia. The next day, media was replaced with Neurobasal media (Neurobasal [Invitrogen], L-glut [Invitrogen], B27 [Invitrogen], penicillin/streptomycin [Invitrogen], doxycycline [2 μg/ml], BDNF [10 ng/ml] [PeproTech], GDNF [20 ng/ml] [PeproTech], and Ara-C). Media was half-exchanged every 3–4 days.

Cell Quantification and Immunofluorescence

Reprogramming efficiency for MEF-iN cell generation was calculated as average percentages of TauEGFP cells per total number of cells (calculated from DAPI stain) in a 20× field of view using an inverted microscope (DMI6000B, Leica). For immunofluorescence staining, cells were washed with PBS and then fixed with 4% paraformaldehyde for 15–20 min at room temperature. Cells were permeabilized and blocked in 0.1% Triton X-100 (Sigma) and 5% cosmic calf serum (CCS) in PBS for 30 min. Primary and secondary antibodies were diluted in a solution of PBS containing 5% CCS. Cells were placed in the primary antibodies overnight at 4°C, washed twice after 8–10 hr with PBS, and then incubated with the secondary antibody for 30 min. The cells were washed three more times with PBS after secondary incubation. Images were acquired using an upright microscope (DM5500B, Leica). Antibodies used were mouse anti-MAP2 (Sigma, 1:500), mouse anti-TUJ1 (Covance, 1:1000), mouse anti-NEUN (Millipore, 1:100), E028 rabbit anti-Synapsin (Südhof lab, 1:500), rabbit anti-vGLUT1 (Synaptic Systems, 1:1000), mouse anti-vGAT (Synaptic Systems, 1:500), chicken anti-GFP (Aves Labs, 1:1000) and Alexa 488- and Alexa Fluor 555-conjugated secondary antibodies (Invitrogen).

Quantifications for vGLUT1-immunoreactivity were performed using ImageJ software. Cells with vGLUT1/vGAT-immunofluorescence intensity >200-fold of background intensity were considered to be positively stained and were normalized to the total TauEGFP-positive cell count for each 20× field view.

Electrophysiology

Electrophysiology experiments were performed similarly to those described before (Chanda et al., 2013). In brief, Tau-EGFP-positive MEF-iN cells, mESC-derived iN cells, or EGFP-infected TTF/HFF/HPF/hESC-iN cells only with elaborate morphological complexity were patched using internal solution containing (for voltage clamp, in mM) 135 $CsCl_2$, 10 HEPES, 1 EGTA, 1 Na-GTP, and 1 QX-314 (pH 7.4, 310 mOsm) or (for current clamp, in mM) 130 $KMeSO_3$, 10 NaCl, 10 HEPES, 2 $MgCl_2$, 0.5 EGTA, 0.16 $CaCl_2$, 4 Na_2ATP, 0.4 NaGTP, and 14 Tris-creatine phosphate (pH 7.3, 310 mOsm). The extracellular solution contained (in mM) 140 NaCl, 5 KCl, 2 $CaCl_2$, 1 $MgCl_2$, 10 glucose, and 10 HEPES-NaOH (pH 7.4). Current-clamp recordings for AP-generation experiments were performed at around −60 mV by using a small holding current to adjust the membrane potential accordingly. Voltage-clamp recordings for AMPAR- and GABAR-mediated responses were made at a holding potential of −70 mV, whereas NMDA-receptor-mediated EPSCs were measured at +40 mV. The pharmacological agents were picrotoxin (50 μM, Tocris), CNQX (25 μM, Tocris), TTX (a voltage-gated Na^+-channel blocker, 1 μM; Ascent Scientific), and tetraethylammonium and 4-aminopyridine (TEA and 4AP, voltage-gated K+-channel blockers, 10 mM and 1 mM, respectively; Tocris). The puff application of 50 μM AMPA (R-S AMPA hydrobromide, Tocris) and GABA (γ-aminobutyric acid, Tocris) was performed for 100 ms using a Picospritzer III (Parker Instrumentation).

Data Presentation

All average data are presented as bar graphs indicating means ± SEM (SD of parameter tested/square root of number of cells

recorded). In most cases, individual parameters measured from individual cells were plotted as color-coded open circles and presented along with average values. The number of cells qualitatively representing a population (a) among total number of cells patched (b) is indicated as a/b, for example traces provided in Figures 4 and 5.

Quantitative RT-PCR

A total of 200 ng of total RNA was reverse transcribed into cDNA using the first Strand cDNA Synthesis kit (Life Technologies) with SuperScript II reverse transcriptase. Template cDNA was amplified using SYBR Master Mix, and quantitative RT-PCR was carried out on the AB7900HT (Life Technologies). Relative quantity (RQ) values were calculated by the delta-delta Ct ($RQ = 2^{-[\Delta Ct_{sample} - \Delta Ct_{control}]}$) method. *Gapdh* was used to normalize the expression levels of each sample (ΔCt), and rtTA-infected MEF samples were used as calibration control. Primer information for individual assay is provided in Supplemental Information 1.

Single-Cell Gene Expression Analysis

Single-cell gene expression profiling was performed using the Fluidigm Biomark dynamic array according to the manufacturer's protocol (Pang et al., 2011). Primers used were taken from Zhang et al. (2013). Sequence information for additional primers used (*SYB1* and *SYB2*) is provided in Supplemental Information 1. To ensure the specificity of the amplification, titrations of total human brain RNA were included in each experiment, and only primers that demonstrated a linear amplification were analyzed. We collected the cytoplasm of single iN cells (28–45 days after transduction) growing on coverslips in 24-well plates by aspiration into patch pipettes. Cytoplasm was ejected into 2X cells-direct buffer (Invitrogen), flash frozen, and kept at −80°C until processing. Thawed cytoplasm was subjected to target-specific reverse transcription and 18 cycles of PCR preamplification with a mix of primers specific to the target genes (STA). STA products were then processed for real-time PCR analysis on Biomark 96:96 Dynamic Array integrated fluidic circuits (Fluidigm). We used custom-designed primetime assays (IDT) to detect specific transcripts. Primers were validated by performing quantitative RT-PCR via Fluidigm platform on different RNA concentrations to generate standard curves for each primer set. Primer efficiency was calculated by the following formula: efficiency = $(10^{-1}/\text{slope})^{-1} \times 100$. Primers within the efficiency range of 85%–115% and slopes between −3.0 and −3.7 were used. Clustering analysis was performed with ΔCt values ($Ct_{GAPDH} - Ct_{gene}$) of corresponding genes using the statistical software R.

SUPPLEMENTAL INFORMATION

Supplemental Information includes three figures and Information 1 and can be found with this article online at http://dx.doi.org/10.1016/j.stemcr.2014.05.020.

AUTHOR CONTRIBUTIONS

S.C. and M.W. conceived the project and designed the experiments; S.C., C.E.A., J.D., C.P., M.M., Q.Y.L., H.A., and S.W.J. performed the experiments and analyzed data; S.C. organized the figures; S.C., T.C.S. and M.W. wrote the manuscript; and all authors commented on the manuscript.

ACKNOWLEDGMENTS

C.E.A. was supported by a California Institute of Regenerative Medicine training grant (TGR-01159), J.D. by a Child Health Research Institute postdoctoral fellowship (Lucile Packard Foundation, UL1-TR001085), C.P. by a fellowship from the National Institute of Child Health and Human Development (1F32HD078051-01), M.M. by a fellowship from the German Research Foundation (DFG), Q.Y.L. by the Agency for Science, Technology and Research (A*STAR, Singapore), and H.A. by a fellowship from the Swedish Research Council and the Swedish Society for Medical Research. This study was funded by NIH grants R01 MH092931 and AG010770-18A1 (to M.W. and T.C.S.). M.W. is supported by the Tashia and John Morgridge Faculty Scholar Fund, Child Health Research Institute at Stanford and a New York Stem Cell Foundation-Robertson Investigator Award.

Received: January 13, 2014
Revised: May 28, 2014
Accepted: May 30, 2014
Published: July 3, 2014

REFERENCES

Baloh, R.H., Enomoto, H., Johnson, E.M., Jr., and Milbrandt, J. (2000). The GDNF family ligands and receptors - implications for neural development. Curr. Opin. Neurobiol. *10*, 103–110.

Bertrand, N., Castro, D.S., and Guillemot, F. (2002). Proneural genes and the specification of neural cell types. Nat. Rev. Neurosci. *3*, 517–530.

Blanpain, C., Daley, G.Q., Hochedlinger, K., Passegué, E., Rossant, J., and Yamanaka, S. (2012). Stem cells assessed. Nat. Rev. Mol. Cell Biol. *13*, 471–476.

Caiazzo, M., Dell'Anno, M.T., Dvoretskova, E., Lazarevic, D., Taverna, S., Leo, D., Sotnikova, T.D., Menegon, A., Roncaglia, P., Colciago, G., et al. (2011). Direct generation of functional dopaminergic neurons from mouse and human fibroblasts. Nature *476*, 224–227.

Cau, E., Casarosa, S., and Guillemot, F. (2002). Mash1 and Ngn1 control distinct steps of determination and differentiation in the olfactory sensory neuron lineage. Development *129*, 1871–1880.

Chanda, S., Marro, S., Wernig, M., and Südhof, T.C. (2013). Neurons generated by direct conversion of fibroblasts reproduce synaptic phenotype caused by autism-associated neuroligin-3 mutation. Proc. Natl. Acad. Sci. USA *110*, 16622–16627.

Clarke, L.E., and Barres, B.A. (2013). Emerging roles of astrocytes in neural circuit development. Nat. Rev. Neurosci. *14*, 311–321.

Fode, C., Ma, Q., Casarosa, S., Ang, S.L., Anderson, D.J., and Guillemot, F. (2000). A role for neural determination genes in specifying the dorsoventral identity of telencephalic neurons. Genes Dev. *14*, 67–80.

Guillemot, F., Lo, L.C., Johnson, J.E., Auerbach, A., Anderson, D.J., and Joyner, A.L. (1993). Mammalian achaete-scute homolog 1 is

required for the early development of olfactory and autonomic neurons. Cell *75*, 463–476.

Han, S.S., Williams, L.A., and Eggan, K.C. (2011). Constructing and deconstructing stem cell models of neurological disease. Neuron *70*, 626–644.

Helms, A.W., Battiste, J., Henke, R.M., Nakada, Y., Simplicio, N., Guillemot, F., and Johnson, J.E. (2005). Sequential roles for Mash1 and Ngn2 in the generation of dorsal spinal cord interneurons. Development *132*, 2709–2719.

Jaenisch, R., and Young, R. (2008). Stem cells, the molecular circuitry of pluripotency and nuclear reprogramming. Cell *132*, 567–582.

Johnson, J.E., Birren, S.J., and Anderson, D.J. (1990). Two rat homologues of Drosophila achaete-scute specifically expressed in neuronal precursors. Nature *346*, 858–861.

Kim, E.J., Battiste, J., Nakagawa, Y., and Johnson, J.E. (2008). Ascl1 (Mash1) lineage cells contribute to discrete cell populations in CNS architecture. Mol. Cell. Neurosci. *38*, 595–606.

Ladewig, J., Mertens, J., Kesavan, J., Doerr, J., Poppe, D., Glaue, F., Herms, S., Wernet, P., Kögler, G., Müller, F.J., et al. (2012). Small molecules enable highly efficient neuronal conversion of human fibroblasts. Nat. Methods *9*, 575–578.

Ladewig, J., Koch, P., and Brustle, O. (2013). Leveling Waddington: the emergence of direct programming and the loss of cell fate hierarchies. Nat. Rev. Mol. Cell Biol. *14*, 225–236.

Lo, L.C., Johnson, J.E., Wuenschell, C.W., Saito, T., and Anderson, D.J. (1991). Mammalian achaete-scute homolog 1 is transiently expressed by spatially restricted subsets of early neuroepithelial and neural crest cells. Genes Dev. *5*, 1524–1537.

Marchetto, M.C., and Gage, F.H. (2012). Modeling brain disease in a dish: really? Cell Stem Cell *10*, 642–645.

Pang, Z.P., Yang, N., Vierbuchen, T., Ostermeier, A., Fuentes, D.R., Yang, T.Q., Citri, A., Sebastiano, V., Marro, S., Südhof, T.C., and Wernig, M. (2011). Induction of human neuronal cells by defined transcription factors. Nature *476*, 220–223.

Parras, C.M., Schuurmans, C., Scardigli, R., Kim, J., Anderson, D.J., and Guillemot, F. (2002). Divergent functions of the proneural genes Mash1 and Ngn2 in the specification of neuronal subtype identity. Genes Dev. *16*, 324–338.

Pfisterer, U., Kirkeby, A., Torper, O., Wood, J., Nelander, J., Dufour, A., Björklund, A., Lindvall, O., Jakobsson, J., and Parmar, M. (2011). Direct conversion of human fibroblasts to dopaminergic neurons. Proc. Natl. Acad. Sci. USA *108*, 10343–10348.

Sugimoto, Y., Furuno, T., and Nakanishi, M. (2009). Effect of NeuroD2 expression on neuronal differentiation in mouse embryonic stem cells. Cell Biol. Int. *33*, 174–179.

Thoma, E.C., Wischmeyer, E., Offen, N., Maurus, K., Sirén, A.L., Schartl, M., and Wagner, T.U. (2012). Ectopic expression of neurogenin 2 alone is sufficient to induce differentiation of embryonic stem cells into mature neurons. PLoS ONE *7*, e38651.

Tucker, K.L., Meyer, M., and Barde, Y.A. (2001). Neurotrophins are required for nerve growth during development. Nat. Neurosci. *4*, 29–37.

Vierbuchen, T., and Wernig, M. (2011). Direct lineage conversions: unnatural but useful? Nat. Biotechnol. *29*, 892–907.

Vierbuchen, T., and Wernig, M. (2012). Molecular roadblocks for cellular reprogramming. Mol. Cell *47*, 827–838.

Vierbuchen, T., Ostermeier, A., Pang, Z.P., Kokubu, Y., Südhof, T.C., and Wernig, M. (2010). Direct conversion of fibroblasts to functional neurons by defined factors. Nature *463*, 1035–1041.

Wapinski, O.L., Vierbuchen, T., Qu, K., Lee, Q.Y., Chanda, S., Fuentes, D.R., Giresi, P.G., Ng, Y.H., Marro, S., Neff, N.F., et al. (2013). Hierarchical mechanisms for direct reprogramming of fibroblasts to neurons. Cell *155*, 621–635.

Wu, D.C., Ré, D.B., Nagai, M., Ischiropoulos, H., and Przedborski, S. (2006). The inflammatory NADPH oxidase enzyme modulates motor neuron degeneration in amyotrophic lateral sclerosis mice. Proc. Natl. Acad. Sci. USA *103*, 12132–12137.

Yamamizu, K., Piao, Y., Sharov, A.A., Zsiros, V., Yu, H., Nakazawa, K., Schlessinger, D., and Ko, M.S. (2013). Identification of Transcription Factors for Lineage-Specific ESC Differentiation. Stem Cell Rev. *1*, 545–559.

Yoo, A.S., Sun, A.X., Li, L., Shcheglovitov, A., Portmann, T., Li, Y., Lee-Messer, C., Dolmetsch, R.E., Tsien, R.W., and Crabtree, G.R. (2011). MicroRNA-mediated conversion of human fibroblasts to neurons. Nature *476*, 228–231.

Zhang, Y., Pak, C., Han, Y., Ahlenius, H., Zhang, Z., Chanda, S., Marro, S., Patzke, C., Acuna, C., Covy, J., et al. (2013). Rapid single-step induction of functional neurons from human pluripotent stem cells. Neuron *78*, 785–798.